Available online at www.sciencedirect.com
SCIENCE DIRECT®
ELSEVIER
European Journal of Mechanics B/Fluids 23 (2004) 475–490
EUROPEAN JOURNAL OF MECHANICS B/FLUIDS

Mesoscale plasma dynamics, transport barriers and zonal flows: simulations and paradigms

A. Thyagaraja [a], P.J. Knight [a], N. Loureiro [b]

[a] *EURATOM/UKAEA Fusion Association, Culham Science Centre, Abingdon, OX14 3DB, UK*
[b] *Plasma Physics Group, Imperial College of Science, Technology and Medicine, London SW7 2BZ, UK*

Received 30 January 2003; received in revised form 30 June 2003; accepted 30 October 2003

Abstract

Tokamaks are magnetic confinement fusion devices which seek to produce power from fusion reactions between the isotopes of hydrogen (deuterium and tritium). The understanding of turbulent transport processes which govern the energy, momentum and current distributions in tokamak plasmas is important to optimising the economically viable design of future power plants based on the tokamak concept. With the advent of powerful modern computers it has become possible to model the plasma dynamics on the so-called "mesoscale" which consists of electromagnetic turbulence with wavelengths intermediate to the ion gyro radius and the system size of typical tokamaks. This paper attempts to describe one such approach which evolves the two-fluid model of a tokamak plasma globally (i.e., both on the macroscale and the mesoscale), using a nonlinear, electromagnetic, three-dimensional code CUTIE. Recent researches, both theoretical and experimental, on tokamaks indicate the spontaneous (or, externally induced) generation of so-called "zonal flows", which, under well-defined conditions, can lead to substantial reduction of turbulent transport in localized regions known as transport barriers. This type of confinement enhancement is of great importance in the design and construction of practical fusion power plants and has been the subject of intensive study. In addition to the computational approach based on CUTIE simulations, we also describe some simpler paradigmatic models which are designed to illustrate the genesis of zonal flows by characteristic drift wave fluctuations and the effects of such highly sheared advective flows on the system dynamics. These models help one to understand in a much clearer fashion the rather complex processes simulated by CUTIE.

1. Introduction

Tokamaks are devices which are designed to confine very hot ($T \simeq 10^8$ K) plasmas by a combination of external and internally produced magnetic fields forming nested tori called 'magnetic flux surfaces' (Nb.: The following references give accessible overviews of recent plasma physics researches related to tokamaks: [1–3]). They are strongly driven, dissipative systems associated with transport rates across flux surfaces of particles, momentum and energy far exceeding predictions based on Coulomb collisional transport. There is a substantial body of experimental evidence [4–7] which suggests that such relatively large transport rates are associated with electromagnetic plasma turbulence.

A crucial problem in building economically viable fusion power plants is the need to understand and control this 'anomalous' (i.e., turbulent) transport. Modern theoretical approaches to tokamak transport have been based on the use of powerful computer codes extending analytic theories of instability mechanisms (see, for example, [8–13]). Fluids and plasmas differ primarily due to the presence of strong electromagnetic fields and kinetic effects associated with high temperatures. In recent years [13,14] a systematic computational approach to the analysis and estimation of turbulent transport has been developed, based on the "two-

E-mail address: a.thyagaraja@ukaea.org.uk (A. Thyagaraja).

0997-7546/$ – see front matter
doi:10.1016/j.euromechflu.2003.10.009

fluid" [15] model of quasineutral plasma dynamics. The purpose of this paper is to give an outline of this approach [13,14] to the simulation and analysis of 'mesoscale' tokamak plasma turbulence phenomena. The mesoscales are characterized by wavelengths intermediate between the ion Larmor radius ($\simeq$1 mm) and the system size ($\simeq$1 m) and time-scales intermediate between the Alfvén time ($\simeq$1–10 ns) and the confinement time ($\simeq 0.1$–10 s). We note that the aim here is to simulate *global* (i.e., including both macro and mesocales) evolution phenomena observed in tokamak experiments.

We also attempt to elucidate the current understanding of so-called 'internal transport barriers' (ITB's), which are regions of substantially *reduced* transport caused (in part) by turbulence-generated flows (usually termed "zonal flows", these are the result of electric fields within the plasma and drifts caused by them in the presence of confining magnetic fields) [5,13,16]. The control of such regions could significantly enhance the potential of future tokamak power plants. Our simulations illustrate the fact that tokamak plasma turbulence is governed largely by the complex spectral interplay between zonal flows, sheared magnetic fields and electromagnetic fluctuations driven by gradients and saturated by nonlinear effects. These dynamical processes are thought to be mediated by interactions involving "direct" (i.e., low to high wave number/frequency) and "inverse" (high to low wave number/frequency) spectral energy cascades. Several simple, but instructive models [17–19] have been used to explicate the nature of these detailed processes. A brief discussion of the main conclusions from these analyses is also provided.

The paper is arranged as follows: in Section 2 we formulate the CUTIE model and state the assumptions underlying its construction. Section 3 is devoted to an overview of the code and the numerical procedures employed. In Section 4 we present some typical simulation results obtained with the help of CUTIE for the conditions of the RTP experiment [6,20] which has provided a wealth of diagnostic detail for comparison with the computations. Section 5 takes up the description of two simpler models for zonal flow generation and their possible effects. These paradigms have been investigated both numerically and analytically. The results are reviewed here and put in context. We present some conclusions in Section 6.

2. Modelling mesoscale tokamak turbulence: key assumptions and equations of motion

The dynamics of a tokamak plasma is governed by Maxwell's equations and Newtonian conservation laws of electrons/ions, momentum and energy. The two-fluid model represents a simplified approach to the complete nonlinear plasma dynamics of the system which neglects several kinetic effects, but seeks to describe in some detail, the physics governing the mesoscales (and the larger macroscales). There are many strong analogies between this model and the traditional fluid dynamical theories based on the Navier–Stokes equations in aerodynamics [21], and more importantly, in meteorology. As in these earlier theories, the key problems revolve around the need to simulate a very large number of dynamical degrees of freedom of a driven, dissipative system, taking into account complex geometrical features and issues associated with boundary conditions, atomic physics processes and kinetic (i.e., velocity space-dependent) considerations.

Given present computational resources, the only *practically* feasible approach to modelling mesoscale tokamak turbulence over time-scales which are long enough to describe evolutionary details remains the two-fluid approximation. In the future, as parallel computing achieves maturity, reliability and speed, it may be possible to adopt a "microscale" approach based on much more detailed kinetic models. It should also be noted that any model, however detailed, has to be compared with experiment in the last analysis. Measurements of turbulent fluctuations in high temperature plasmas are still in their infancy and detailed theoretical predictions are often not directly comparable with currently measurable observables. For example, it is not yet feasible to measure, in sufficient detail, the turbulent electromagnetic fields *within* the plasma. The situation is not unlike that in condensed matter theory, where microscopic theories are rarely of practical use in describing real materials and one resorts to "semi-phenomenological" models such as the Ginzburg–Landau theory.

In the two-fluid theory [12,13] (in the following, we use Gaussian CGS units which render comparisons with earlier works easier), the electron and ion fluids are described by their (common) number density, $n_e \simeq n_i = n$, temperatures, $T_{e,i}$ (in ergs), the plasma flow velocity $\mathbf{v}$, the magnetic field $\mathbf{B}$ and the electrostatic potential, ϕ. It is well known [22] that provided one is interested in length-scales much greater than the Debye shielding length (λ_{Debye}) and frequencies small compared with the electron plasma frequency (ω_{pe}), the electron and ion number densities are constrained by "quasineutrality", which implies, for hydrogen plasmas, the relation, $n_i \simeq n_e$. Here the plasma frequency and the Debye length are related to more familiar properties by, $\omega_{\mathrm{pe}}^2 = 4\pi n_e e^2/m_e$, where $-e$ is the electron charge in Gausssian units, m_e is the electron mass and $\lambda_{\mathrm{Debye}} = v_{\mathrm{the}}/\omega_{\mathrm{pe}}$, where $v_{\mathrm{the}} = (2T_e/m_e)^{1/2}$. Electromagnetic turbulence in the mesoscale invariably satisfies the necessary conditions for quasineutrality to be a relatively good approximation. This also means that Maxwell's displacement current may be neglected and the plasma current density satisfies "Ampère's Law", $\mathbf{j} = \frac{c}{4\pi}\nabla \times \mathbf{B}$. To avoid misunderstanding, we are here considering *turbulence*. For *wave propagation* of high frequency electromagnetic waves, it is *crucial* to include the displacement current. The quasineutrality assumption is analogous (both mathematically and physically) to the familiar "incompressible" flow approximation for low Mach number fluid dynamics [21].

In conventional tokamaks, the 'toroidal' magnetic field is mostly externally produced by appropriate field coils and is much larger than the plasma's own 'poloidal' field (typically, $B_{\mathrm{tor}}/B_{\mathrm{pol}} \simeq 10$). The latter is created generally by the currents driven

within the plasma by externally applied voltages, current drive or certain intrinsic effects due both to collisions (e.g., the so-called "bootstrap current" [1]) and turbulence (e.g., the so-called "dynamo effect" [2]). Typically, the plasma internal energy is smaller than the total magnetic energy, i.e., $\beta = 8\pi p/B^2 \ll 1$, although, power plant economics demands that this parameter should be as large as possible within the constraints of hydromagnetic stability of the system (generally, $\beta \gg (m_e/m_i)$, the electron–ion mass ratio) [1]. Furthermore, the mesoscale turbulent fluctuation frequencies observed experimentally are considerably lower than the ion Larmor/gyro frequency ($\omega_i = eB/m_i c \simeq 10^8$ rads/s) and the wavelengths generally somewhat longer than the ion Larmor/gyro radius, ρ_s ($= (2T/(m_i)^{1/2}/\omega_i \simeq 1$–$10$ mm, where, $T = T_e + T_i$). A characteristic feature of tokamak turbulence is that the wavelengths *parallel* to the local magnetic field are of the order of the system size whilst those in the *perpendicular* directions are considerably smaller (i.e., $k_\parallel \ll k_\perp$).

The equations we use take the standard general forms:

$$\frac{\partial n}{\partial t} + \nabla \cdot (n\mathbf{v}) = S_p, \tag{1}$$

$$m_i n \frac{\mathrm{d}\mathbf{v}}{\mathrm{d}t} = -\nabla p + \mathbf{j} \times \mathbf{B}/c + \mathbf{F}_{\mathrm{eff}}, \tag{2}$$

$$\frac{3}{2}\frac{\mathrm{d}p_{e,i}}{\mathrm{d}t} + p_{e,i}\nabla \cdot \mathbf{v}_{e,i} = -\nabla \cdot \mathbf{q}_{e,i} + P_{e,i}, \tag{3}$$

$$\mathbf{E} + \mathbf{v}_e \times \mathbf{B}/c = -\nabla p_e/en + \mathbf{R}_e, \tag{4}$$

$$\nabla \times \mathbf{B} = 4\pi \mathbf{j}/c. \tag{5}$$

The following definitions hold: $(m_i + m_e)\mathbf{v} = m_i \mathbf{v}_i + m_e \mathbf{v}_e$. This relates the plasma "fluid velocity" vector, $\mathbf{v}$, to the velocity fields of the electrons ($\mathbf{v}_e$) and the ions ($\mathbf{v}_i$). Note that since $m_e/m_i \ll 1$, $\mathbf{v} \simeq \mathbf{v}_i$. The current density is obtained from the obvious relation, $\mathbf{j} = en(\mathbf{v}_i - \mathbf{v}_e)$. Typically, although there are exceptions, the electrons carry most of the current in a tokamak. It is convenient to split the total magnetic field, $\mathbf{B} = \nabla\psi \times \mathbf{b}_\mathrm{t} + B_0 \mathbf{b}_t$, where $\mathbf{b}_\mathrm{t}$ is the unit vector in the "toroidal" direction. The electric field is given by, $\mathbf{E} = -\frac{1}{c}\frac{\partial \psi}{\partial t}\mathbf{b}_\mathrm{t} - \nabla\phi$, and the plasma pressure, $p = p_e + p_i = n(T_e + T_i)$. The external particle source is represented by S_p, whilst the effective force on the plasma is taken to be $\mathbf{F}_{\mathrm{eff}}$. The electron–ion friction force is $\mathbf{R}_e$, whilst $\mathbf{q}_{e,i}$ are the heat-flux vectors.

A brief description of the physics content of the above equations is useful. Eq. (1) evidently describes particle balance, allowing for external particle sources like gas puffing and pellets. Eq. (2) describes momentum balance. The LHS represents the plasma inertia (mainly due to the ions). The first term on the RHS is the scalar pressure gradient force, the second term is the Lorentz force, whilst the third term contains both collisional and turbulent viscous effects. It can, in principle, also include external momentum inputs due to neutral beams, charge-exchange and/or radio frequency waves (i.e., "ponderomotive forces"). While gravity can be important in astrophysical problems, its effects are negligible for tokamak physics.

One needs to specify constitutive relations for $\mathbf{F}_{\mathrm{eff}}$ in order to close the system at this level. These can be empirical or based on experiment or more detailed kinetic models (cf. [15]). Note that the ideal magnetohydrodynamic ("Ideal MHD") approximation of this equation simply consists of dropping this last term. Eqs. (3) represent a pair of "energy balance" equations for the two species and are differential expressions of the Laws of Thermodynamics in the continuum limit. The LHS terms are well known from ordinary fluid dynamics. Many complications of plasma physics arise from the extreme anisotropy and complicated forms taken by the heat flux vectors, $\mathbf{q}_{i,e}$ and the energy sources/sinks embodied in $P_{i,e}$ (cf. [13,15]). Eq. (4) is effectively a statement of the momentum balance of the *electron fluid*. Electrons can be treated as massless in tokamak physics, so long as the length-scales of interest are not shorter than the so-called "electron skin depth", $c/\omega_{\mathrm{pe}} \simeq \rho_s (m_e/m_i)^{1/2}\beta^{-1/2} \simeq 0.1\rho_s$. In our model, electron inertia is neglected, as inclusion of this effect would only be justified with considerably higher spatial resolution than practicable at present. The resultant partial differential equation is often termed the "generalized Ohm's Law", and is one of the key equations of the model, incorporating various electron drift effects (as before, the "friction force", $\mathbf{R}_e$ on the electrons has to be specified by suitable constitutive relations [13,15]). The final equation (5) is an expression of quasineutrality and provides the means to compute the plasma current density, $\mathbf{j}$ in terms of the spatial derivatives of the $\mathbf{B}$, ψ.

3. Reduction of the equations in the tokamak approximation and solution method

In the CUTIE turbulence code, the tokamak is represented by a 'periodic cylinder', where the polar coordinate, θ, represents the 'poloidal' angle and $\zeta = z/R$ is the 'toroidal' angle. The flux surfaces are labelled by the cylindrical radial coordinate, r. This approximation is relevant when the "inverse aspect ratio", $\varepsilon = a/R$ of the device is small. It has been widely used in the literature as a good working basis for tokamak analyses. As the main interest in our model is turbulence dynamics, it *is* important to include certain geometrical effects due to field line curvature [1,15]. This is indeed done to a first approximation in

the ordering parameter ε. The representation of the electric field in terms of the two potentials, ϕ, ψ given above also follows from "tokamak ordering": in this, the magnetic field fluctuations *parallel* to the equilibrium field are neglected compared to the fluctuations in the r, θ (or "poloidal") plane. It then turns out that Eq. (4) can be manipulated to lead to an evolution equation for ψ and an expression for $\mathbf{v}_\perp$ in terms of ϕ. By some other reductions, one obtains an evolution equation for the "potential vorticity" which is related to ϕ. For the purpose of completeness, the equations of motion governing the dynamical evolution of the *fluctuating components* of ϕ and ψ are given below.

We first introduce nondimensional dependent variables and apply the decomposition, $f(r,\theta,\zeta,t) = f_0(r,t) + f^*(r,\theta,\zeta,t)$, where the (position space) "fluctuation amplitudes", f^* are not necessarily small, but do depend on both angular variables. We then develop them, using the double Fourier series:

$$f^* = \sum_{m=-\infty}^{\infty} \sum_{n=-\infty}^{\infty} \hat{f}_{m,n}(r,t) \exp(\mathrm{i}m\theta + \mathrm{i}n\zeta). \tag{6}$$

By definition, the 'mean' $f_0(r,t)$ represents the $m = n = 0$ Fourier component of the variable $f(r,\theta,\zeta,t)$, and consequently, $\hat{f}_{0,0} \equiv 0$. Since all plasma fields considered are real, the Fourier coefficients satisfy the reality condition, $\hat{f}_{m,n} = \bar{\hat{f}}_{-m,-n}$, where the over-bar denotes complex conjugation. The electromagnetic fields are described in terms of two potentials, ϕ and ψ. These are *fluctuating* parts(thus, $\delta\mathbf{E} = -\nabla\phi - \frac{1}{c}\frac{\partial\psi}{\partial t}\mathbf{e}_\zeta$; note that, $\mathbf{e}_\zeta \equiv \mathbf{b}_\mathrm{t}$). The corresponding 'mean' quantities are denoted by, $\Phi_0(r,t)$, $\Psi_0(r,t)$.

It should be clear that there is no length or time-scale separation implied in writing (for example) $n = n_{e0}(r,t) + \delta n_e(r,\theta,\zeta,t)$. Formally, the "equilibrium" and the "fluctuation" equations are together equivalent to the complete two-fluid conservation equations (1)–(5). The first term is merely the $m = 0$, $n = 0$ Fourier component of the complete electron density field. It is convenient to separate it out from the fluctuations (solved in the Fourier space), and solve the position-space "transport equation" which governs it. The second, fluctuation term contains in principle, all other Fourier modes. The first term is indeed forced by explicit external sources (particle source, for example) but also "feels" the flux surface averages of the turbulent fluxes which are explicitly incorporated in the evolution equations for the equilibrium. These latter can (and generally do) fluctuate rapidly in time and in r (compared with the inverse confinement time and the system size, a). For this reason, quantities like $n_{e0}(r,t)$, and more particularly their gradients can develop "fine structure" which we term corrugations. These back react on the turbulence and have profound consequences for the evolution of the system as a whole as exemplified by our results.

We should make it clear that CUTIE models *both* the "mesoscale" and the macroscale and their mutual interactions self-consistently. Indeed, the mesoscale variations crucially affect and are in turn back-reacted by the macroscales. In this respect, CUTIE differs decisively from simulations which calculate turbulent fluctuations (linearly or nonlinearly) whilst keeping the background driving gradients like $\mathrm{d}T_i/\mathrm{d}r$, $\mathrm{d}j/\mathrm{d}r$, $\mathrm{d}p/\mathrm{d}r$ *fixed*.

The following dimensional parameters occur naturally in the theory: the "Alfvén velocity", $\overline{V}_A^2 = B_0^2/4\pi m_i n(0,t)$; the "sound velocity", $\overline{V}_\mathrm{th}^2 = (T_e(0,t) + T_i(0,t))/m_i$; "ion gyrofrequency", $\omega_{ci} = eB_0/m_i c$; "effective gyroradius", $\rho_s = \overline{V}_\mathrm{th}/\omega_{ci}$; "plasma beta", $\beta = (\overline{V}_\mathrm{th}/\overline{V}_A)^2$. In addition, we introduce the 'potential vorticity' (with dimensions, $[1/T]$), $\Theta = \nabla\cdot(\frac{n_0(r,t)}{n_0(0,t)}\nabla_\perp\frac{c\phi}{B_0})$. We also define the nondimensional fluctuations, ϕ^*, ψ^*, Θ^*:

$$\frac{c\phi}{B_0} = \overline{V}_\mathrm{th}\rho_s\phi^*, \quad \frac{\psi}{B_0} = \rho_s\beta^{1/2}\psi^*, \quad \Theta = \frac{\overline{V}_\mathrm{th}}{\rho_s}\Theta^*, \quad \Theta^* = \rho_s^2\nabla\cdot\left(\frac{n_0(r,t)}{N^*}\nabla_\perp\phi^*\right),$$
$$n^* = \frac{\delta n_e}{N^*}, \quad \lambda_{i,e}^* = \frac{\delta T_{i,e}}{T^*}, \quad \xi^* = \frac{n_0(r,t)\delta v_\parallel}{\bar{\xi}},$$

where, $N^* = n_e(0,t)$, $T^* = T_e(0,t) + T_i(0,t)$, and $\bar{\xi} = N^*\overline{V}_\mathrm{th}$. Note that we nondimensionalize only the *dependent* variables. In principle, lengths can be made nondimensional using either the system size (e.g., "minor radius", a) or the typical Larmor radius, ρ_s. Similarly, the time can be made made nondimensional using either the Alfvén time, $\tau_A = a/\overline{V}_A$, or the "sound time", $\tau_s = a/\overline{V}_\mathrm{th}$. The problem inherently depends upon *both* meso and macroscales, and it is useful *not* to render the independent variables nondimensional.

The system is thus described completely by these variables and the corresponding 'mean' quantities, which are conveniently chosen to be, $n_0(r,t)$, $T_{e0}(r,t)$, $T_{i0}(r,t)$, $v_{\theta 0}(r,t)$, $v_{\zeta 0}(r,t)$, $E_{r0}(r,t)$, $B_{\theta 0}(r,t)$. Several different advection velocities occur in the theory. By definition, $E_{r0} = -\partial\Phi_0/\partial r$. The velocity, $\mathbf{u}_0 = -(cE_{r0}/B)\mathbf{e}_\theta + \mathbf{b}_0 v_{\parallel 0}$ represents the equilibrium 'MHD' flow of the plasma (ions), whilst $\mathbf{u}_{e0}$ represents the corresponding electron flow, $\mathbf{u}_{e0} = -(cE_{r0}/B)\mathbf{e}_\theta + \mathbf{b}_0(v_{\parallel 0} - j_{\parallel 0}/en_0)$. The ion fluid flow (i.e., MHD flow + diamagnetic flow) is given by, $\mathbf{v}_0 = \mathbf{u}_0 + (c/(en_0B))(\partial p_{i0}/\partial r)\mathbf{e}_\theta$. We also have the relation, $\Theta_0 = \frac{1}{r}\frac{\partial}{\partial r}((rn_0(r,t)/N^*)(c/B_0)\partial\Phi_0/\partial r)$. Finally, $\mathbf{v}_{e0} = -[cE_{r0}/B + c/(en_0B)\partial p_{e0}/\partial r]\mathbf{e}_\theta$ is the total electron *poloidal flow* composed of the electron $\mathbf{E}\times\mathbf{B}$ equilibrium flow and the electron diamagnetic flow. In the following, $\nabla_\parallel \equiv \mathbf{b}_0\cdot\nabla = \frac{1}{qR}(\partial/\partial\theta + q\partial/\partial\zeta)$ (i.e., the gradient in the direction of the *unperturbed field*). The nonlinear terms account for the exact field direction.

The equations of motion governing the spatio–temporal evolution of the electromagnetic fluctuations, with these conventions, are the following:

$$\Theta^* = \rho_s^2 \nabla \cdot \left(\frac{n_0}{N^*} \nabla_\perp \phi^* \right), \tag{7}$$

$$\begin{aligned} \frac{\partial \Theta^*}{\partial t} + \mathbf{v}_0 \cdot \nabla \Theta^* + \overline{V}_A \nabla_\parallel \rho_s^2 \nabla_\perp^2 \psi^* &= \overline{V}_A \rho_s \frac{1}{r} \frac{\partial \psi^*}{\partial \theta} \frac{4\pi \rho_s}{c B_0} j_0' + \overline{V}_{\rm th} \rho_s \frac{1}{r} \frac{\partial (\psi^*, \rho_s^2 \nabla_\perp^2 \psi^*)}{\partial (r, \theta)} \\ &+ \overline{V}_{\rm th} \rho_s \left[\frac{1}{r} \frac{\partial (\Theta^*, \phi^*)}{\partial (r, \theta)} + \left(\frac{N^* T_{i0}}{n_0 T^*} \right) \frac{1}{r} \frac{\partial (\Theta^*, n^*)}{\partial (r, \theta)} \right] - \frac{2 \overline{V}_{\rm th} \rho_s}{R_0} \left[\frac{\cos\theta}{r} \frac{\partial p^*}{\partial \theta} + \sin\theta \frac{\partial p^*}{\partial r} \right] + \rho_s^2 \Theta_0' \frac{1}{r} \frac{\partial \phi^*}{\partial \theta} + \Sigma_\Theta^*, \end{aligned} \tag{8}$$

$$\frac{\partial \psi^*}{\partial t} + \mathbf{v}_{e0} \cdot \nabla \psi^* + \overline{V}_A \nabla_\parallel \phi^* = \overline{V}_A \left(\frac{N^* T_{e0}}{n_0 T^*} \right) \nabla_\parallel n^* + \overline{V}_{\rm th} \rho_s \left[\frac{1}{r} \frac{\partial (\psi^*, \phi^*)}{\partial (r, \theta)} - \left(\frac{N^* T_{e0}}{n_0 T^*} \right) \frac{1}{r} \frac{\partial (\psi^*, n^*)}{\partial (r, \theta)} \right] + \Sigma_\psi^*. \tag{9}$$

The fluctuating source terms on the RHS contain self-consistent turbulent diffusion terms dependent on the local fluctuating potential vorticity and current density. Thus, typically, $\Sigma_f^* \simeq \nabla \cdot D_{\rm turb} \nabla f^*$, for the fluctuating quantity, f^*. Here, $D_{\rm turb}$ is taken proportional to Θ^*, $\rho_s^2 \nabla_\perp^2 \psi^*$, the highest spatial derivatives of ϕ^*, ψ^* in the system. It is analogous to eddy diffusivity terms familiar from aerodynamics and meteorology. These sinks are needed to provide the "high wave number cut off" required to prevent well known undesirable (and unphysical) aliasing effects and Gibbs phenomena associated with truncated Fourier series. Physically, there are many effective collisional and kinetic mechanisms which provide a strong sink at high wave numbers. In an "exact" model, one would be using a physical cutoff. In reduced models such as the two-fluid theory, it is usual to employ simpler forms based on physical intuition. The basic idea is that if too much enstrophy (fluid and magnetic) piles up at the high k of the modelled fluctuations, the turbulent eddy diffusivity must dissipate it by a self-consistent process. The principle behind such a turbulence-dependent eddy viscosity reflects the fact that the direct cascade is actually driven by modulational instabilities of the low-k spectrum and therefore the flux in k-space to the short wavelengths and the dissipation rate at the subgrid range must depend on those amplitudes. We monitor the values of this quantity during the simulations and find that they invariably remain smaller than typical constant eddy viscosities of the "Bohm diffusion" type. The eddy viscosity we employ will be vanishingly small if the system happens to be locally linearly stable, for instance (as in an ITB). The actual forms used and the complete set of equations including those for n^*, $\lambda_{i,e}^*$, ξ^* can be found in [13].

It is worth noting that the above equations contain some very fundamental and robust physics. The equations (Eqs. (7), (8)) for ϕ^* are simply consequences of the quasineutrality condition, $\nabla \cdot \mathbf{j} = 0$, Newton's laws and the "generalized Ohm's Law", Eq. (3). Indeed, exactly similar equations also result in the more familiar "ideal MHD" approximation, where, the Ohm's Law is greatly simplified and takes the form, $c\mathbf{E} + \mathbf{v} \times \mathbf{B} = 0$. The equation for ψ^* (Eq. (9)) has an even more direct provenance: it represents the combination of Faraday's Law of Induction and the generalized Ohm's Law in the toroidal direction. These equations and the corresponding ones for the plasma properties ($n^*, \lambda_{e,i}^*, \xi^*$) are believed to contain the essential macro-scale modes in a tokamak. They do *not* describe some subtle kinetic effects (e.g., collisonless, "Landau damping" [22]) due to velocity-space distributions and those arising from particle-trapping, which are the most important of the many kinetic effects. They also do not contain the "fast" magnetosonic wave, which can only be modelled by greatly enlarging the model.

The above equations must be supplemented by the evolution equations governing the "mean potentials" ($\Phi_0(r,t), \Psi_0(r,t)$), and those relevant to n^*, $\lambda_{e,i}^*$ etc. It suffices to sketch the general structure of the mean equations. Let $f_0(r,t)$ be a typical "mean" (e.g., particle density). It can be easily deduced from the full equations of motion by taking the $m = 0$, $n = 0$ Fourier component (equivalently averaging over an equilibrium flux surface, r), that this evolves according to,

$$\frac{\partial f_0}{\partial t} = -\frac{1}{r} \frac{\partial}{\partial r} \left[r \Gamma_f(r,t) \right] + S_f(r,t). \tag{10}$$

Here, Γ_f represents the *total* flux of the quantity f across the flux surface. In general, this flux is due to transport processes due to collisions which are present even in the absence of turbulence, as well as turbulence-induced fluxes. Thus, one may write generally, $\Gamma_f \equiv \Gamma_f^{\rm coll} + \Gamma_f^{\rm turb}$. The fluxes, $\Gamma_f^{\rm coll}$ include the so-called "classical" and "neoclassical" terms [1,15], which can be advective and/or diffusive and may also involve both f_0 and its radial gradients as well as other fields, such as temperatures, etc. Within the fluid model, turbulent fluxes are mainly advective ones, due essentially to the fluctuating $\mathbf{E} \times \mathbf{B}$ drifts across the flux surfaces. These take the general form,

$$\Gamma_f^{\rm turb} = \langle \delta V_r f^* \rangle = \frac{1}{4\pi^2} \int_0^{2\pi} \int_0^{2\pi} \delta V_r(r, \theta, \zeta, t) f^*(r, \theta, \zeta, t) \, {\rm d}\theta \, {\rm d}\zeta, \tag{11}$$

where δV_r is the turbulent radial ($\mathbf{E} \times \mathbf{B}$) velocity fluctuation and f^* is the fluctuating part of f. Note that the average in question is *not* a time-average, but one over the equilibrium flux surface at r. In principle, these turbulent components *can* and do vary

rapidly, i.e., on the "fast" turbulent length (in the radial direction) and time-scales. This term is crucial in introducing local, mesoscale "corrugations" in $f_0(r,t)$. In the special case of electrons, the large *parallel* heat transport implies, in the presence of turbulence, an effective *radial* transport (i.e., $\langle \mathbf{q}_{\|e} \rangle$ can make a substantial contribution to the heat flux across equilibrium surfaces). This purely *electromagnetic transport* has been investigated by many authors (e.g., [23]), following the early work of Kadomtsev and Pogutse [24] and Rechester and Rosenbluth [25]. The source, S_f is also the effective surface averaged source derived from the full equations of motion. It too is, in general composed of all the mean effects as well as turbulent fluctuations. A full discussion of these issues and constitutive properties would take us too far afield.

It is useful to summarise briefly the methods used to solve the above coupled system of nonlinear partial differential equations. More details are available in [13]. As far as the fluctuations are concerned, the boundary conditions employed are relatively straightforward. Regularity near the magnetic axis, $r = 0$ implies that the fluctuation fields must tend to zero near this real singular point (it is a poloidal field null, the only one in the periodic cylinder model). The plasma "edge" is actually arranged to be at $r/a = 0.95$. It is therefore permissible and practical to set all fluctuations to zero at $r/a = 1$. The periodicity with respect to the angles is already taken into account by the Fourier representation. Since radial diffusion (collisional or turbulent) is always present, the two radial boundary conditions are necessary and sufficient. In the case of the mean quantities, typically, the radial derivative is set to zero at $r = 0$ and a small, physically appropriate "pedestal" edge value applies at $r = a$. The fluctuation equations for the variables, ϕ^*, ψ^*, Θ^*, n^*, λ_e^*, λ_i^*, ξ^* can be written in the general symbolic form:

$$\frac{\partial \mathbf{X}}{\partial t} = \mathbf{L}(\mathbf{X}) + \mathbf{N}(\mathbf{X}), \tag{12}$$

where $\mathbf{X}$ denotes a column vector of the above dependent variables, $\mathbf{L}$ is a linear parabolic operator which, in general, mixes the fields and depends upon the "mean" quantities as well as the *poloidal angle*, θ, but *not* the toroidal angle ζ. The nonlinear operator, $\mathbf{N}$ involves $\mathbf{X}$ quadratically as well as the corresponding mean quantities. These operators may also explicitly depend upon r, θ and t, although not ζ. It is clear that Eqs. (7)–(9) already suggest this general form. Adding the evolution equations for the remaining dynamical variables does not modify the structure. Both $\mathbf{L}$ and $\mathbf{N}$ may depend upon spatial derivatives of $\mathbf{X}$ up to second order. The second order derivatives always occur linearly. The nonlinear terms have "conservation" properties typical of the Jacobians in the governing equations. It should be noted that elliptic effects are also involved in our system, since Eq. (7) is effectively a "Poisson" equation for ϕ^* when the "potential vorticity", Θ^* is known everywhere in the solution domain.

This general structure is exploited in the pseudo-spectral, semi-implicit, iterative numerical scheme used to advance the fields in time. At any time-step, using the (known) current values of $\mathbf{X}$ and the corresponding mean quantities, the nonlinear terms are evaluated in position space using the position space representation of the variables. This evaluation uses a second-order, conservative Arakawa scheme to evaluate various Jacobeans. Then, the equations are Fourier transformed in the angles and finite-differenced with second order accuracy in r. One then obtains systems of one-dimensional parabolic equations for each Fourier mode m, n over the radial domain. The *linear* operator $\mathbf{L}$ is in principle inverted by a radial block-tridiagonal scheme based on Gaussian elimination (it is thus a *direct* method). The time-advancement uses a predictor–corrector iterative scheme. Thus, the linear modes are *implicitly* treated and the nonlinear terms are re-evaluated at each iteration, for each Fourier mode, using the Fast Fourier Transform algorithm.

For instance, denoting by $\mathbf{X}_i(m,n,t+\Delta t)$, the column vector formed by these five Fourier components (of the variables, Θ^*, ϕ^*, ψ^*, n^*, ξ^*; $\lambda_{i,e}^*$ are obtained by a separate solution, as detailed below) at the radial mesh point (i), the resultant system of (nonlinear) algebraic equations takes the form,

$$\mathbf{A}_i^0 \mathbf{X}_i(m,n,t+\Delta t) = \mathbf{A}_i^+ \mathbf{X}_{i+1}(m,n,t+\Delta t) + \mathbf{A}_i^- \mathbf{X}_{i-1}(m,n,t+\Delta t) + \mathbf{S}_i, \tag{13}$$

where $\mathbf{A}_i^0$, $\mathbf{A}_i^+$, $\mathbf{A}_i^-$ are (5×5) complex matrices (functions of m, n, i, t) and $\mathbf{S}_i$ is a 'source' column vector including nonlinear and toroidal coupling effects as well as terms involving $\lambda_{i,e}^*$. The semi-implicit differencing scheme (centred-space, backwards time for implicit terms and centred time for the explicit ones) ensures that this block-tridiagonal system is always invertible (i.e., non-singular) for $\mathbf{X}_i$ at $t+\Delta t$, given the values at t and the boundary conditions. This linear system is inverted by complex block-tridiagonal, Gauss–Jordan pivoting for $-m_{\max} \leqslant m \leqslant m_{\max}$ and $0 \leqslant n \leqslant n_{\max}$. Reality conditions are used to determine the values for the remaining n harmonics. Having obtained $\mathbf{X}_i$, the semi-implicitly differenced, Fourier-transformed versions of the energy equations are solved by a radial block-tridiagonal (2×2) matrix solver for $\hat{\lambda}_{i,e}(r_i,m,n,t+\Delta t)$. The complete solution involves two predictor–corrector iterations at each time-step. Extensive experience with both linear and nonlinear simulations has shown that the scheme described is stable and convergent. The prescription of the time-step is limited by accuracy considerations, with $V_A \Delta t/a \simeq 0.25$, being a typical choice. Spatial resolutions are chosen to obtain, $\Delta r \leqslant \rho_s$, at least, away from the cool edge.

This procedure is relatively stable and has been bench-marked against known linear instabilities. It requires the storage of three-dimensional arrays of the fluctuations both in position space *and* Fourier space at the "current time", t and the "new time", $t+\Delta t$. At each iteration, the corresponding *mean* equations are solved using the latest estimates of the fluctuations and the fluxes they imply in the mean equations. The cost of this is essentially the same as solving for a single (m,n) Fourier mode. The

iterations at a time-step need not be large, provided the step length is small enough to resolve the principal turbulence frequencies of interest ($\leqslant$1 MHz typically, with $\Delta t \simeq 50$ ns). Indeed, the scheme yields converged results as the mesh is successively refined, up to the point when the equations of the model cease to represent the physics at the grid scales. The reader is referred to the review by Thyagaraja [13] which discusses many of these technical points in greater detail.

4. Mesoscale evolution of tokamaks: CUTIE simulations and experiments

Experiments in the RTP tokamak [6] suggest that the 'safety factor', $q = rB_t/RB_p$ which measures the pitch of the magnetic field lines plays an important role in the formation and dynamics of ITB's. In the RTP experiment, when the plasma is heated using electron–cyclotron resonance heating (350 kW ECH), it was found that when the deposition radius crossed plasma surfaces with low rational values of q, the central temperatures varied in 'steps', as if 'quantized'. These results could be phenomenologically represented by an advection–diffusion model called the 'q-comb' model, in which the effective thermal diffusivity varied with q in a step-like manner [6]. This was indicative of certain barrier phenomena associated with electron transport.

Simulations using CUTIE [13] show that long wavelength electromagnetic turbulence generated near such 'rational surfaces' helps to 'self-organize' the plasma and acts to reduce the transport locally, leading to ITB's close to rational surfaces located near the deposition radius. The current density and vorticity of the flows are also found to be radially highly 'structured' or 'corrugated' [13]. CUTIE also accounts for significant advective transport effects indicated by experiment. The observations show that when the electron heating is 'off-axis', the temperature profile has an *off-axis maximum* (see Fig. 1 where experimental points are indicated by open triangles). Remarkably, CUTIE simulations reproduce (cf. Fig. 1, solid line) these results semi-quantitatively and indicate outward *advection* near the axis to be the key effect. It is readily shown that if the electron heat flux were purely *diffusive*, in the absence of sinks in the central region (ruled out by the experimentalists after carefully estimating all other causes), it is impossible for the temperature profile to be "hollow" as observed experimentally. CUTIE simulations suggest the existence of long wavelength modes to be the cause of the outward advective heat loss within the heating radius. The CUTIE code has been applied to study the *evolution* of tokamak discharges under a variety of conditions in the RTP tokamak and other machines. These investigations are on going and have been reported in detail elsewhere [28]. An interesting class of RTP experiments in which radio frequency power source is *modulated* and the tokamak response measured, is reported by Mantica et al. in [20]. In these experiments, the idea is to switch on and off an electron cyclotron heating source in a well-defined manner. Thus the power is kept on for 2.8 ms and switched off for 400 ms at the same deposition radius. This corresponds to a "duty cycle" of 85% and period of 312 Hz. The temperature profiles are measured with adequate spatio–temporal resolution and the response of the plasma to this *periodic heat source* can be analysed. By these means the time-averaged (over many cycles) electron temperature profile and the fundamental and first two Fourier (time) harmonics of the temperature have been analysed [20]. In particular, the behaviour of the amplitudes and relative phases enable one to discuss the effects of transport barriers. Using CUTIE, we have simulated some of the experiments discussed by Mantica et al.

Considering a case where the heating was applied at the deposition radius, $\rho_{dep} \equiv r/a = 0.44$ (350 kW, other plasma conditions are set close to the experimental ones) we show, in Fig. 2, the calculated variation of the electron temperature as a

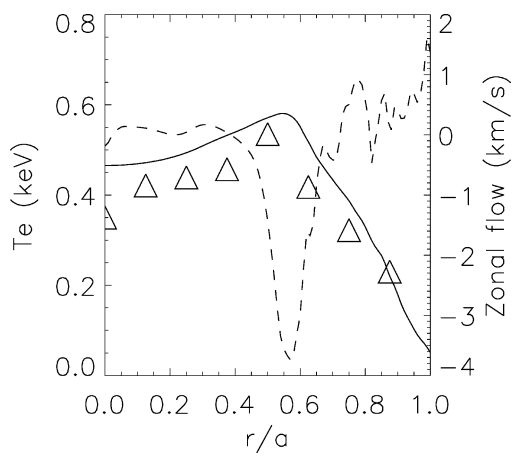

Fig. 1. RTP simulation: $P_{ECH} = 350$ kW at $r/a = 0.55$. Simulated T_e (solid line), V_{zonal} (dotted line) profiles are shown. Experimental T_e values are indicated by △.

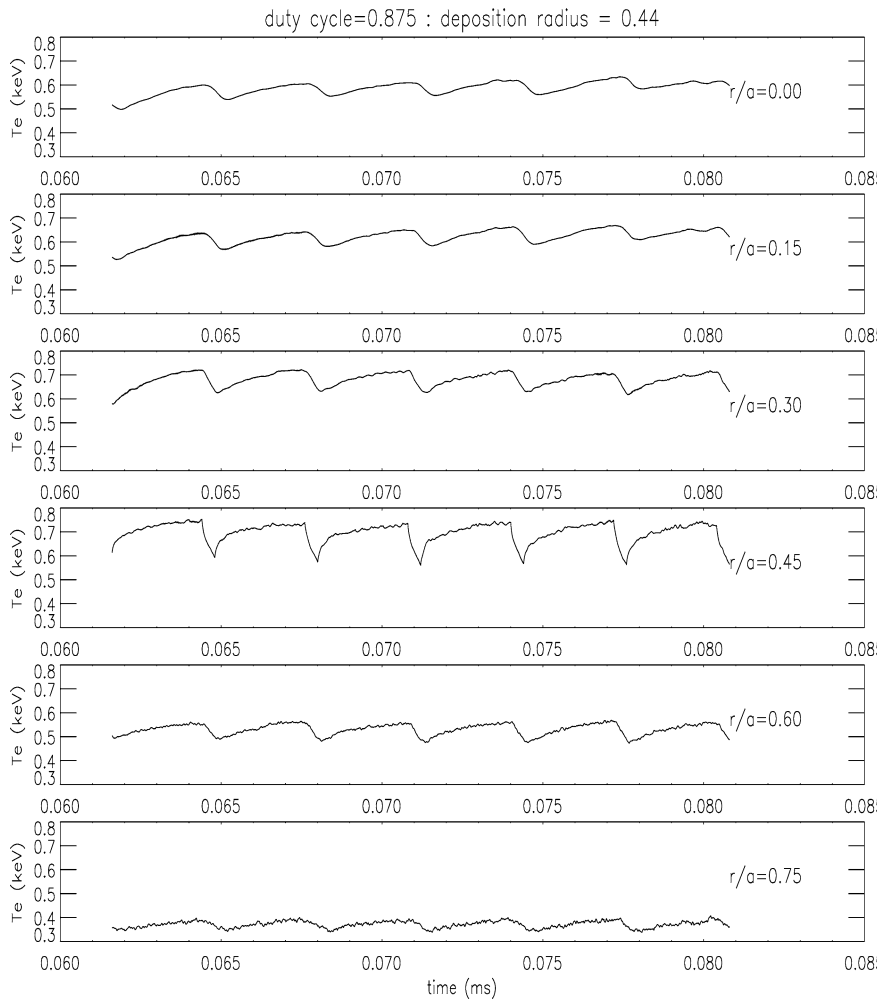

Fig. 2. RTP modulated heating simulation: $P_{\mathrm{ECH}} = 350$ kW at $r/a = 0.44$. Simulated T_e responses at different radii are shown (see text for details).

function of time and r/a. It is seen that plasma response is "anharmonic" close to the deposition radius, tending to be sinusoidal further in and out. The perturbations tend to die out faster for $r/a > 0.44$ as compared with inner locations. The profile, $T_e(r, t)$ is Fourier analysed (both in the experiment and in the simulations) with respect to time. Of particular interest are the time-averaged (or mean) profiles and the Fourier coefficients at ω, 2ω, 3ω, where $\omega/2\pi = 312$ Hz, the modulation frequency. These latter profiles are conventionally referred to as the "harmonics".

The time-averaged T_e profile and the first three harmonics (from the simulations) are shown to scale in Fig. 3. The first harmonic extends well into the central core. In Fig. 4(a) we show the first three harmonic amplitudes profiles. The maximum amplitude of the first harmonic (i.e., "fundamental") is about 45 eV, somewhat smaller than the experimental value of 60 eV (Fig. 4 in [20]). The calculated second and third harmonic amplitudes agree rather better with experiment. The code does not however get the inward shift of the maximum of the first harmonic, seen in experiment (op. cit, Fig. 4). Furthermore, in the experiment, the fundamental does not decay as expected from energy conservation (as seen in the simulations; see, Fig. 4(a)) for $r/a > 0.44$. The reasons for the discrepancy are not understood. However, the relative phases of the perturbations in the simulations (see Fig. 4(b)) agree reasonably well with those measured.

In summary, the evolutionary behaviour of tokamaks subject to time-dependent sources (and sinks when laser ablated pellets are used to send "cold pulses" into steady discharges) are being studied using CUTIE. Generally the simulations appear to lead to qualitative agreement with experiment, at least in small devices like RTP. This area is under intense investigations, especially concerned with transport barrier physics in the Joint European Torus, JET, where experiments have revealed the role played by both the q profile and zonal flows [7].

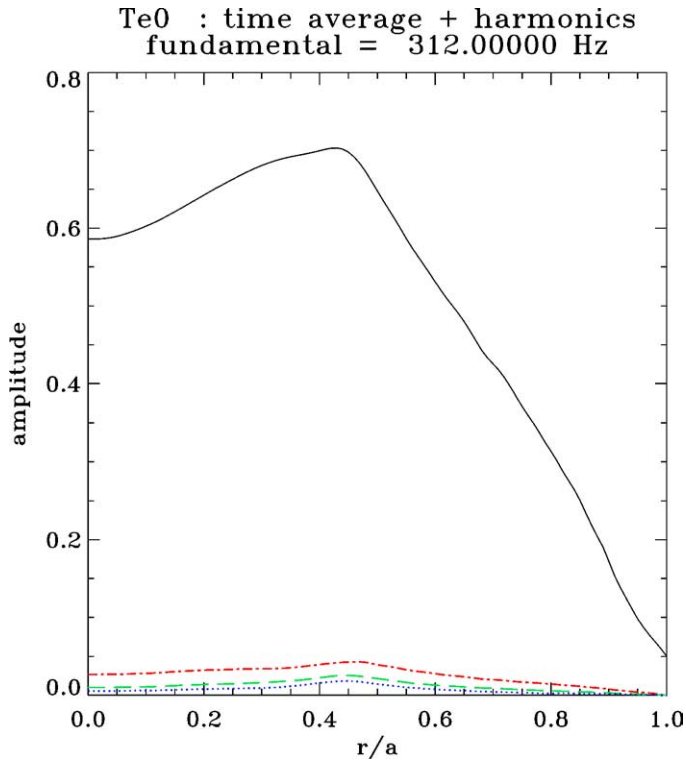

Fig. 3. RTP modulated heating simulation: time-averaged T_e (solid) first three Fourier harmonics (keV) (see text for details).

The code also reproduces mesoscale instabilities qualitatively (the most important of these are the so-called drift modes driven by temperature gradients and electromagnetic modes driven by current and pressure gradients), as illustrated by movies made from the solutions. It is known from other experimental data (see references in Ref. [13]) that the radial component of the electric field plays a key role in suppressing turbulence locally. Such fields lead to $\mathbf{E} \times \mathbf{B}$ plasma flows in the poloidal (i.e., θ) direction. If strongly sheared, these flows act to decorrelate the turbulent fluctuations which transport particles and energy across the flux surfaces (see [2] and references therein). CUTIE simulations demonstrate that highly radially 'corrugated' poloidal flows can be spontaneously generated by the turbulence via an "inverse cascade" (see Fig. 1 for the 'jet-like' zonal flow profile close to heating radius obtained from CUTIE). They also show that these flows do indeed tend to locally suppress the turbulent transport.

There are two separate issues which arise in connection with the dynamics of zonal flows and their interactions with plasma turbulence: firstly, it is desirable to construct a generic model based on drift-wave physics which explicitly exhibits the generation of "zonal flows" by drift waves; secondly, one seeks to have a *simple* explanation of the effects due to a highly sheared transverse flow on the *radial transport* of turbulence and fluxes. A brief outline of investigations which seek to answer these questions is given in the next section.

5. Paradigmatics of zonal flows

The equations solved by CUTIE are, in spite of many simplifying assumptions, rather complicated. As stated at the end of the previous section, it is desirable to have a model for understanding the genesis of zonal flows by turbulent fluctuations. Such a model was studied by one of the authors and co-workers [19]. The model consists of the so-called Generalized Charney–Hasegawa–Mima equation (GCHME), which is a simplified, conservative nonlinear partial differential equation in two spatial dimensions. Unlike the two-fluid equations solved by CUTIE, GCHME is dissipationless. It possesses small amplitude drift-wave solutions when linearized about a suitable, exact, steady state. The equation is also known to be a model of Rossby waves in geophysics [18]. It describes the time-evolution of the electrostatic potential, $\phi(x, y, t) = \bar{\phi}(x, t) + \tilde{\phi}(x, y, t)$, where $\bar{\phi}$ denotes the "mean" potential, related to the zonal flow velocity, $V_{0y} = \frac{c}{B}\bar{\phi}_x$. Here, c denotes the speed of light, and B is the magnetic field (assumed uniform and constant) along the z-axis. The subscript denotes the "radial" derivative. The fluctuation potential

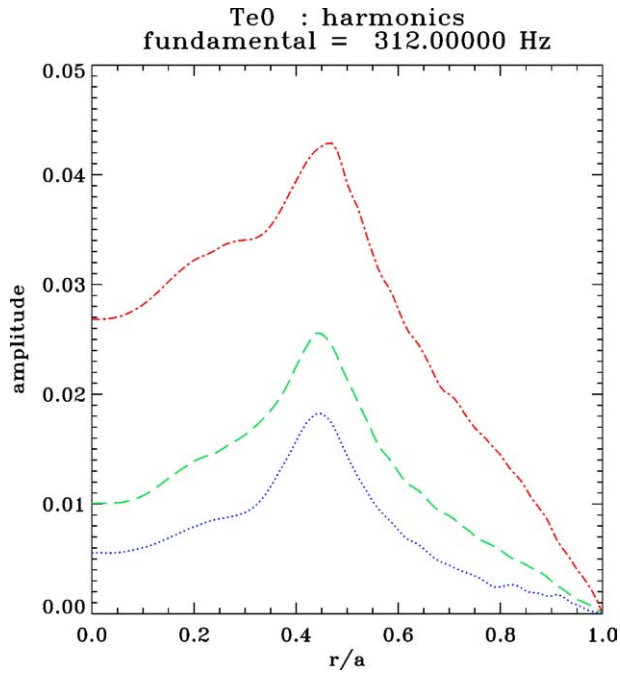

(a)

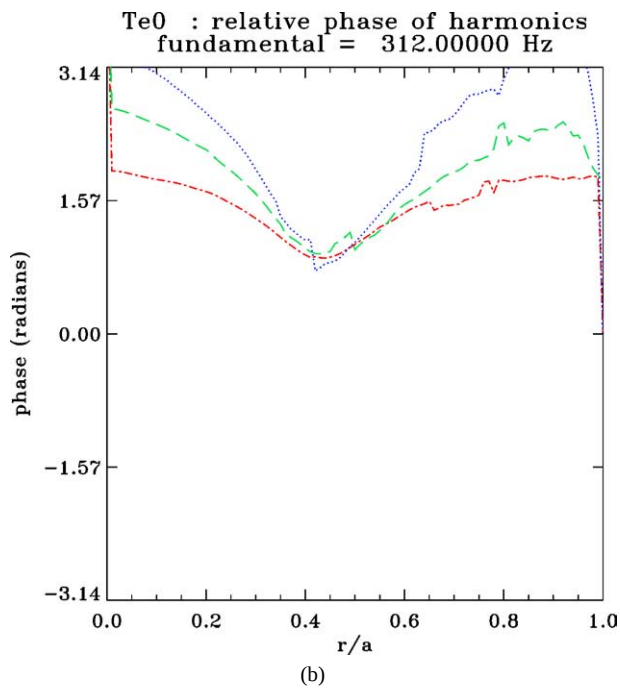

(b)

Fig. 4. RTP modulated (312 Hz) heating simulation: (a) T_e harmonics (keV), (b) relative phases (radians): red-312 Hz, green-624 Hz, blue-936 Hz.

is $\tilde{\phi}$, depending on both x and y. All quantities are taken to be periodic in these directions, except for the equilibrium electron number density, $\bar{n}$, which is assumed to vary with x over a length-scale, L_n ($L_n^{-1} \equiv \frac{1}{\bar{n}(x)}|\frac{\mathrm{d}\bar{n}}{\mathrm{d}x}|$). The electron temperature, T_e is assumed uniform and constant, whilst the ions are taken to be "cold" (i.e., their temperature is neglected in comparison with T_e).

With these conventions, $\mathbf{V}_0 = V_{0y}\mathbf{y}$ is the y-averaged $\mathbf{E}\times\mathbf{B}$ drift (this will be consistently referred to in this paper as the 'zonal flow'), whilst $\widetilde{\mathbf{V}}_E = c\mathbf{z}\times\nabla\tilde{\phi}/B$ represents the fluctuating $\mathbf{E}\times\mathbf{B}$ drift, and $\mathbf{V}_d = V_d\mathbf{y}$ is the diamagnetic drift. We set $\rho_s = c_s/\Omega_{ci}$, and $c_s = (2T_e/m_i)^{1/2}$, $\Omega_{ci} = eB/m_i c$, $V_d = c_s\rho_s/L_n$. Here, m_i is the ion mass.

The nonlinear behaviour of the electrostatic potential is then described by the GCHME

$$\left(\frac{\partial}{\partial t} + \mathbf{V}_0\cdot\nabla + \mathbf{V}_d\cdot\nabla\right)\frac{e\tilde{\phi}}{T_e} - \left(\frac{\partial}{\partial t} + \mathbf{V}_0\cdot\nabla + \widetilde{\mathbf{V}}_E\cdot\nabla\right)\rho_s^2\nabla_\perp^2\frac{e\phi}{T_e} = 0. \tag{14}$$

In [19] this equation is cast into a non-dimensional form and a pair of coupled nonlinear equations for $\bar{\phi}$, $\tilde{\phi}$ are derived. The equations admit a simple steady solution. Linear perturbations about this "equilibrium" state yield drift waves whose frequency and wave number are given by, $(\omega_0, \mathbf{k}_0)$ where, $\mathbf{k}_0 = (k_x, k_y, 0)$ and,

$$\omega_0 = \frac{\alpha k_y}{1+\hat{\rho}^2 k_0^2}, \tag{15}$$

with,

$$k_0^2 = k_x^2 + k_y^2. \tag{16}$$

where $\alpha = a/L_n$, $\hat{\rho} = \rho_s/a$, and a represents the size of the x domain. It was also shown in the work cited that there are two *exact* integral invariants of the system which depend quadratically on the potential and its spatial derivatives up to second order. These are physically identified with energy and "enstrophy" (i.e., the integrated square of the vorticity, here along the magnetic field). The existence of the integrals guarantees the linear stability of the drift waves at small amplitude, as well as the *nonlinear saturation* of the system after a sufficiently long time starting from an arbitrary initial state. In this respect, the model differs from CUTIE which represents a *driven, dissipative system*.

The key finding of the work can be summarised thus: starting with a *small but finite amplitude* drift-wave with given wave number $\mathbf{k}_0$, ω_0, when its *side bands* with wave numbers, $\mathbf{k}_0 \pm q\mathbf{x}$ are considered, they *beat* with the drift wave and produce a *zonal flow* potential perturbation at a wave number, $\mathbf{q} = q\mathbf{x}$. This is a "degenerate" drift wave with nominally zero frequency, as $k_y = 0$ for zonal flow potentials, $\bar{\phi}$, by definition. It is now possible for the original finite-amplitude drift wave (called the "pump wave") to steadily lose energy due to the "modulationally unstable" trio formed by the zonal flow and the two side bands. Although eventually such an instability *must* saturate when the amplitudes of the side bands become comparable with the pump, the initial phases of the instability can be analysed by linear theory, treating the "pump amplitude" as constant. The criterion for modulational instability can be obtained from the following expression (cf. [19], Eq. (48)) for the growth rate in terms of the initial "pump" amplitude, A_0:

$$\gamma^2 \approx k_y^2\alpha^2 q^2\left(\frac{2A_0^2}{\alpha^2\hat{\rho}^2} - q^2\hat{\rho}^2\right). \tag{17}$$

Reverting to dimensional expressions for clarity, it is clear that the threshold condition on the pump wave is,

$$|A_0|^2 > \frac{\omega_0^2 q^2\hat{\rho}^4}{2k_y^2} > (\rho_s q)^2\frac{V_d^2}{2c_s^2}. \tag{18}$$

Clearly the threshold is very low since $V_d^2 \ll c_s^2$, and $(\rho_s q)^2 \ll 1$. We note that the threshold amplitude is proportional to the 'drift Mach number' defined by, $M_d = |V_d|/c_s$ and to $|q|$.

Since γ^2 is parabolic in q^2, it is straightforward to show that the maximum growth rate occurs for

$$q_{\max} \approx \frac{A_0}{\alpha\hat{\rho}^2}. \tag{19}$$

The threshold condition also implies that for modulational instability, q (the dimensional radial wave number of the zonal flow) must be in the unstable band given by,

$$0 < \rho_s q < \sqrt{2}\frac{c_s}{V_d}|A_0|. \tag{20}$$

Furthermore, the wave number corresponding to maximum growth is,

$$(\rho_s q)_{\max} = \frac{c_s}{V_d}|A_0|. \tag{21}$$

This modulational instability has long been known as the "Benjamin–Feir" instability in fluid mechanics [26] as well as in plasma physics (see also other references cited in [19]).

This model leads to a rather generic mechanism for the spontaneous creation of not only zonal flows (i.e., perturbations of $\bar{\phi}$), but more general *cascade processes* operating in nonlinear systems. In particular, the "inverse cascade" to longer wavelength modes and to zonal flows is more likely to be robust to dissipation, than "direct cascades" to short wavelengths. Work in progress on this model both numerically and analytically confirms this mode of generation of zonal flow by nonlinear "beat" processes, even when there is manifestly no *linear* instability mechanism present to drive zonal flows.

In summary, the numerical and analytical study by Lashmore–Davies et al. [19] of GCHME leads to the following findings: for an initial monochromatic drift wave pump with small but finite amplitude, a modulational instability can occur, characterized by growing zonal flow and sideband perturbations (i.e., a four-wave interaction). The pump threshold for instability is readily satisfied, depending on the zonal flow wave number. The fully nonlinear GCHME is then solved with a numerical scheme, which has been validated by demonstrating the conservation of the two exact invariants. The simulations show that the validity of the four-wave model is limited to approximately three instability growth times. The radial structure of the zonal flow can be "jet-like" or highly oscillatory in radius depending upon the ratio of the system size to the density scale length and initial conditions. It is found that zonal flows can be dramatically reduced if the most unstable zonal flow wave number does not fit into the system. In CUTIE, the equilibrium radial electric field (and consequent zonal flow) is generated by several different mechanisms operating simultaneously and in turn "back-reacts" on the turbulence in complex ways (both linearly and nonlinearly). The paradigm provided by GCHME enables the rather tangled physics of the two-fluid turbulence to be understood in a relatively simple way.

We next turn to the *effects* to be expected when a strongly sheared zonal flows exist in a system. Here again, the consideration of a simple advection–diffusion equation has thrown considerable light on the key issues. Such a model was discussed in detail by the authors in Ref. [17]. The simplest system which exhibits the relevant features shown in the CUTIE simulations of zonal flow effects in turbulence evolution is the 'passive scalar' equation:

$$\frac{\partial f}{\partial t} + v_y(x)\frac{\partial f}{\partial y} = D\frac{\partial^2 f}{\partial x^2}, \tag{22}$$

where f stands for a generic 'fluctuation' amplitude, $v_y(x)$ is a 'sheared zonal flow' and D is a diffusivity (taken spatially uniform for simplicity). The variable x corresponds to "radius" in the CUTIE context, whilst y represents the "poloidal angle", θ. The system is assumed periodic in y and satisfies homogeneous b.c's in a finite slab in $0 \leqslant x \leqslant a$.

Although the model is highly simplified and two-dimensional, the essential physics of the *linear* effects of sheared advection transverse to the difusion can be understood with its use. The spectral properties of this *linear, parabolic equation* have been examined both analytically (in simple but illuminating analytically soluble cases), and numerically. We have used both time-marching and numerical eigenvalue solution methods. The eigenvalue problem is non-selfadjoint, but was discussed in [17] using a contour integral method. When D is small, in the absence of v_y' (i.e., 'Peclet number', $Pe = a^2|v_y'|/D = 0$; in some contexts involving momentum transport, the Peclet number may also be referred to as the Reynolds number), the 'damping rate' of f is proportional to D/a^2. However, in the presence of flow-shear ($Pe \gg 1$), the effective damping rate is proportional to $D^{1/3}$ (i.e., much faster!).

This general conclusion is shown by time-marching solutions of the equation (analogous to the much more complicated CUTIE simulations) as being due to a 'direct cascade' into high radial wave numbers. The sheared advective flow strongly "phase-mixes" in the radial wave number spectrum (transverse to it). This transfers modal energy in the long radial wavelengths to the short wavelengths which are rapidly damped by radial diffusion. In effect, the advection "facilitates" the damping by collisional/diffusive effects by its direct cascading of energy to the very short wavelengths. This process is clearly illustrated in Fig. 5(a)–(c) where we show the time-evolution calculated by the CADENCE time-marching code (cf. [17]). The advection equation is solved by a conservative method setting $D = 0$ in this case. The advection velocity has a simple, constant shearing rate (i.e., vorticity perpendicular to the flow). The direct cascade into the high k_x is clearly seem. Note that in this model we are *not* concerned with *how* the sheared advection might have arisen in the first place, only what happens to quantities (like turbulent fluctuations) which are subject to advective transport. It is, in this sense, complementary to the GCHME described previously.

By a "jet" profile we mean a velocity field that is zero everywhere except in a small region of the domain, where it assumes a high value. Physically, this kind of profile in CUTIE is due to both turbulent Reynolds and Lorentz forces/stresses and corrugations in the ion pressure gradient. In the case of electron physics, current gradients and dynamo effects produce similar changes in advective (i.e., electron inertial) terms involved in "generalized Ohm's Law" which represents electron momentum balance.

We have studied the effect of a profile composed of two of these jets, that is:

$$V(x) = \begin{cases} V_{01}, & x_{01} - \delta < x < x_{01} + \delta, \\ V_{02}, & x_{02} - \delta < x < x_{02} + \delta, \end{cases} \tag{23}$$

where V_{01} and V_{02} are the constant heights of the jets, x_{01} and x_{02} their centres and 2δ the total width of a jet (supposed the same for both jets). Elsewhere $V(x) = 0$. Given that the profile is either zero or constant, solution to the governing advection–

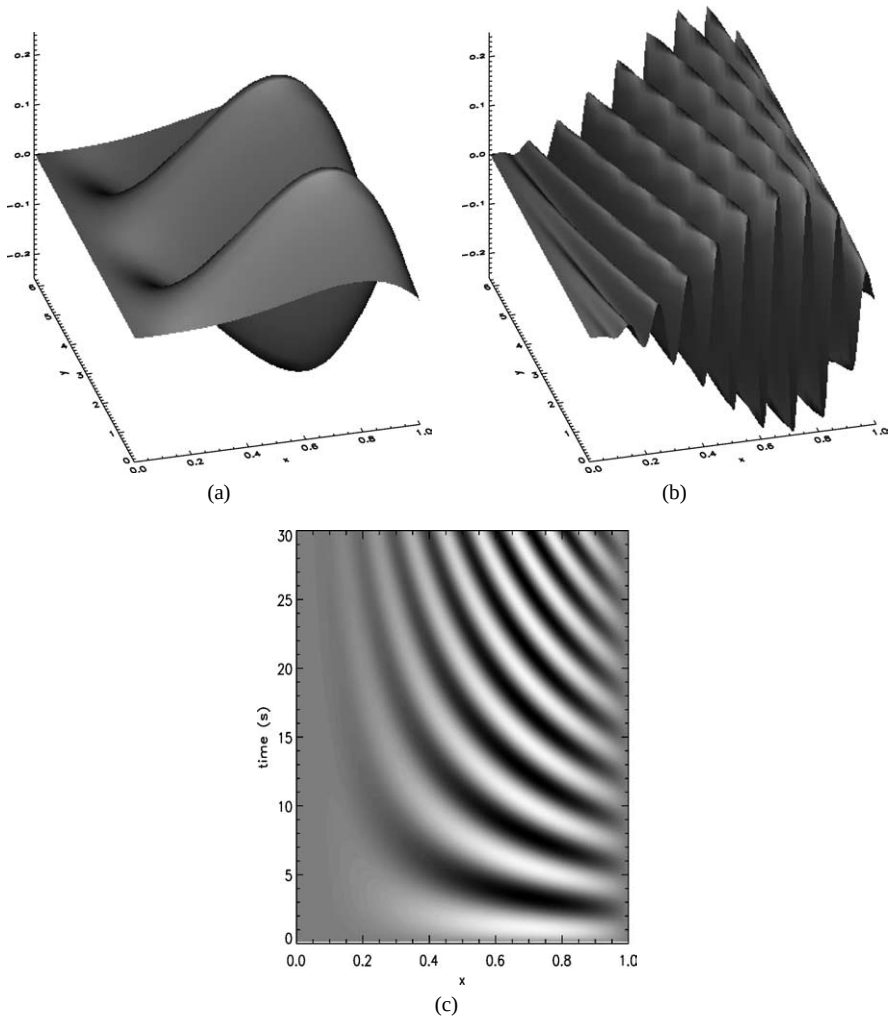

Fig. 5. CADENCE calculation of the evolution of a function $f(x, y)$ with transverse advection $v_y(x) = -x$, in the absence of diffusion. Fig. 5(a) shows initial state of f, Fig. 5(b) that of f at $t = 30$ s, and Fig. 5(c) shows the evolution in time of f at a fixed y. The increase in radial wave number k_x is immediately apparent.

diffusion equation is trivial in each sub-region of the domain. Eigenvalues can thus be obtained by matching solutions from the different regions and using the boundary conditions. Very good agreement was obtained between numerical and analytic eigenvalues.

Main results may be summarised as follows: (1) The spectrum has as many branches as the number of regions into which the domain is divided. (2) Geometric degeneracy occurs if the domain is invariant under rotation/reflection. For example, in the case of a double jet profile, there will be degeneracy if $V_{01} = V_{02}$ and jets are equally spaced from the boundaries of the domain (say, for instance, $x_{01} = 0.35$ and $x_{02} = 0.65$). In this situation there are two obvious ways to remove the degeneracy: either make $V_{01} \neq V_{02}$ or make the distances of the jets' centres to the boundary walls different. In, Fig. 6(a), for example, the real and imaginary parts of the complex frequency eigenvalues are plotted. In this model, the modes are always damped by the combined effect of diffusion and transverse advection. (3) Different regions of the domain are isolated from each other, implying that eigenfunctions will approach zero values near the jets, as can be seen in Fig. 6(b). For high enough Reynolds/Peclet numbers ($R = 10^5$ is already sufficient) eigenfunctions will only exist in one of the three regions in which the jets divide the domain. We have thus found that this kind of velocity profile "confines" the eigenfunctions in the regions between the jets. Each branch of the eigenspectrum stands for one of these regions.

The confinement of the eigenfunctions is an interesting result and should be of importance in the limiting of radial correlations and propagation effects associated with the turbulence. Hence, it may alter the turbulent transport. It is believed that

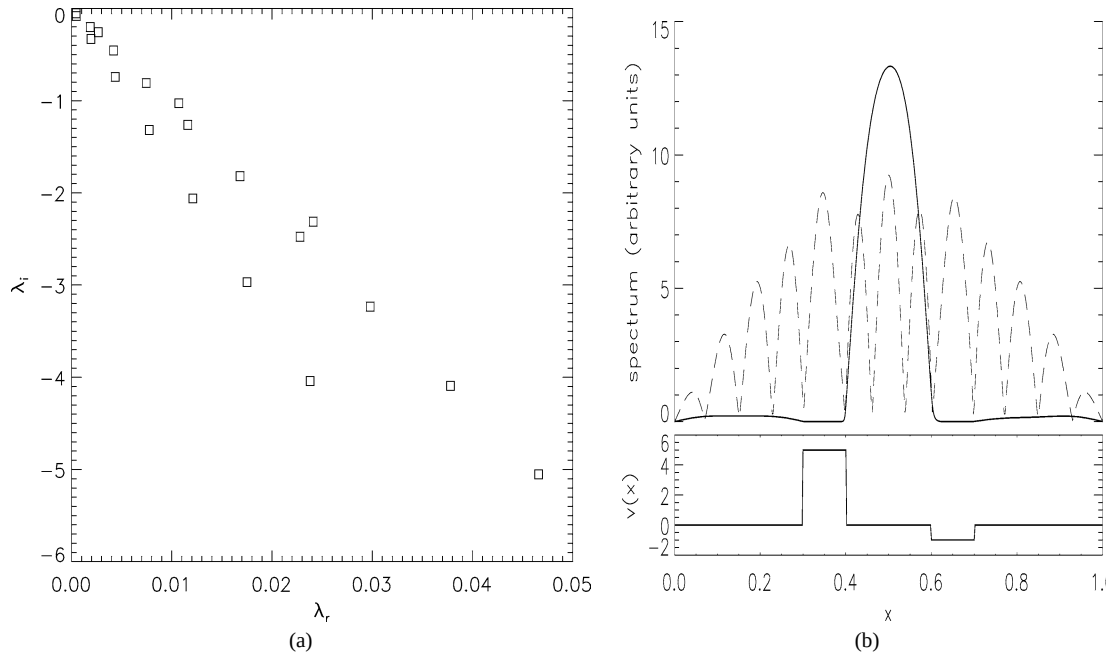

Fig. 6. (a) Double jet spectra: $V_{01} = V_{02} = 500$; $x_{01} = 0.35$; $x_{02} = 0.80$; $\delta = 0.005$. Three independent branches shown: degeneracy is removed by breaking the symmetry of the jets. (b) Time-marching solution of Eq. (22) for a 'jet-like' $v_y(x)$. Dotted line shows f_{init} and solid line f_{fin}, demonstrating 'confinement' by the jets.

this effect may significantly contribute to the "stopping" of radially propagating hot/cold pulses at transport barriers observed in experiment [7] and simulated by CUTIE. Results are obviously generalizable for an arbitrary number of jets. It should be noted that this type of "ghetto-isation" of transported scalars by advection–diffusion equations was already foreshadowed in an astrophysical context in an earlier investigation by Parker and one of the authors [27].

Both simulations and rigorous analysis show that 'jet-like' flows can 'confine' the fluctuations to the zones where they occur (cf. Fig. 6(b)), preventing them from crossing regions of highly sheared flows. These results help understand ITB dynamics predicted by CUTIE qualitatively, as being due to a synergy of electromagnetic effects associated with rational q values (i.e., electron) and zonal flow-shear suppression effects due to electrostatic (i.e., ion) effects. Thus when highly "corrugated" current density and radial electric fields are produced, either by the turbulence itself through "dynamo effects" or "modulational instabilities" (as discussed earlier), or through external current-drives and momentum sources, these electron and ion flows act on the equations governing the fluctuations and help to damp the turbulence by enhancing the capacity of radial diffusion to cause saturation at lower amplitudes than would be possible otherwise. In addition to this purely *linear* (and therefore rather robust mechanism), there is also *nonlinear* radial *decorrelation* caused by the breaking up of the turbulent eddies in the radial direction in to smaller scale structures. This reduction in the radial correlation lengths is one way in which the radial transport due to the turbulent electric fields is reduced. Thus the *direct cascade* into higher radial wave numbers is equivalent to effectively a *smaller* radial step-length, and therefore, of turbulent "diffusion".

It is not yet clear from CUTIE simulations whether it is the linear or nonlinear effect of sheared advective flow which is operative. It is probable that both effects operate simultaneously and synergistically in the "self-organization" process clearly seen in CUTIE simulations of long term evolution.

6. Conclusions

The studies described using CUTIE and the simpler advection–diffusion model lead to the identification of a purely linear, phase-mixing/direct cascade mechanism which amplifies the effect of any viscous or resistive dissipative damping by a self-generated or externally driven, sheared zonal flow (an idea going back to Hasegawa et al. [18] which originally arose from models of the Jovian atmosphere). Coupled with the modulational instabilities of the type exhibited by GCHME, resulting in 'inverse cascades' of plasma turbulence, a quantitative understanding of the principal features of mesoscale tokamak transport

phenomena such as ITB's is beginning to emerge. The assumptions used in CUTIE can be relaxed, although the computational costs of doing so would be usually prohibitive. The approach adopted by the authors (cf. [13,14]) can be succinctly described as "minimalist", in the sense that we only include physical effects in the equations which appear to be crucially important to describe the phenomena discussed. It is possible that a more accurate quantitative model must include many more of the terms and effects neglected in our description. We are primarily interested in discovering the empirically determined limits to which we can take our "reduced" nonlinear electromagnetic model. The advantages of such an "Occam's Razor" philosophy are too obvious to need further justification. Clearly a systematic comparison of results obtained from our model with experiment will, by itself, point to further improvements and future developments. The point of the paper is to pose the question, "*what does the proposed two-fluid model say about mesoscale tokamak turbulence and transport?*", and to describe results which seek to answer it. The key thesis of a turbulence-based theory of tokamak plasma transport like the present model is that the self-consistent determination of plasma properties like f_0, f^* and the electromagnetic field fluctuations leads, for given sources, to a very different plasma evolution than would be obtained when the turbulent components to the fluxes like Γ_f are entirely neglected. Furthermore, the efficacy of any such model should be judged by comparison of the profiles of f_0 and turbulent spectra of f^* predicted by the model subject to the given sources, with experimental observation of the *same quantities*, obtained under similar conditions. While such a program is far from complete at the present time, we have discussed results obtained with the help of our model, which tend to support the claim that it represents a variety of mesoscale phenomena in a tokamak in a qualitative fashion. It is clear that the concepts identified in this study have direct relevance to many other fields such as meteorology and astrophysics where the occurrence of inhomogeneous turbulence is the norm, rather than the exception.

Acknowledgements

The authors have great pleasure in expressing their thanks to their colleagues and collaborators: Drs. Marco de Baar, G.M.D. Hogeweij, Paola Mantica, Howard Wilson and Mr Erik Min. N.L thanks *Fundacao para a Ciencia e a Tecnologia, Ministerio da Ciencia e do Ensino Superior*, Portugal for their support. This research was supported by jointly by the United Kingdom Engineering and Physical Sciences Research Council and EURATOM.

References

[1] B.B. Kadomtsev, Tokamak Plasma: A Complex Physical System, Institute of Physics, Bristol, 1992.
[2] K. Itoh, S.-I. Itoh, A. Fukuyama, Transport and Structural Formation in Plasmas, Institute of Physics, Bristol, 1999.
[3] J.A. Wesson, et al., Tokamaks, second ed., Oxford University Press, Oxford, 1997.
[4] E.J. Strait, et al., Enhanced confinement and stability in DIII-D discharges with reversed magnetic shear, Phys. Rev. Lett. 75 (1995) 4417.
[5] V.V. Parail, Energy and particle transport in plasmas with transport barriers, Plasma Phys. Control. Fusion 44 (5A) (2002) A63.
[6] A.M.R. Schilham, G.M.D. Hogeweij, N.J. Lopes Cardozo, Electron thermal transport barriers in RTP: experiment and modelling, Plasma Phys. Control. Fusion 43 (2001) 1699–1721.
[7] P. Mantica, et al., Perturbative transport experiments in JET low or reverse magnetic shear plasmas, Plasma Phys. Control. Fusion 44 (2002) 2185.
[8] F. Jenko, et al., Electron temperature gradient driven turbulence, Phys. Plasmas 7 (2000) 1904.
[9] B. Scott, $E \times B$ shear flows and electromagnetic gyrofluid turbulence, Phys. Plasmas 7 (2000) 1845.
[10] A. Zeiler, J.F. Drake, B.N. Rogers, Magnetic reconnection in toroidal η_i mode turbulence, Phys. Rev. Lett. 84 (2000) 99.
[11] Z. Lin, et al., Gyrokinetic simulations in general geometry and applications to collisional damping of zonal flows, Phys. Plasmas 7 (2000) 1857.
[12] X.Q. Xu, et al., Low-to-high confinement transition simulations in divertor geometry, Phys. Plasmas 7 (2000) 1951.
[13] A. Thyagaraja, Numerical simulations of tokamak plasma turbulence and internal transport barriers, Plasma Phys. Control. Fusion 42 (2000) B255–B269.
[14] A. Thyagaraja, Global numerical simulations of turbulence and transport in a tokamak, in: Theory of Fusion Plasmas, Proc. Joint Varenna-Lausanne International Workshop, Villa Monastero, Varenna, 1996, p. 155.
[15] R.D. Hazeltine, J.D. Meiss, Plasma Confinement, Addison–Wesley, New York, 1992.
[16] T.S. Hahm, Physics behind transport barrier theory and simulations, Plasma Phys. Control. Fusion 44 (5A) (2002) A87.
[17] A. Thyagaraja, N. Loureiro, P.J. Knight, Spectral and evolutionary analysis of advection–diffusion equations and the shear flow paradigm, part 2, J. Plasma Phys. 68 (2003) 1.
[18] A. Hasegawa, C.G. Maclennan, Y. Kodama, Nonlinear behavior and turbulence spectra of drift waves and Rossby waves, Phys. Fluids 22 (1979) 2122–2129.
[19] C.N. Lashmore-Davies, D.R. McCarthy, A. Thyagaraja, The nonlinear dynamics of the modulational instability of drift waves and the associated zonal flows, Phys. Plasmas 8 (2001) 5121–5133.
[20] P. Mantica, et al., Heat convection and transport barriers in low-magnetic-shear Rijnhuizen Tokamak Project plasmas, Phys. Rev. Lett. 85 (2000) 4534.

[21] L.D. Landau, E.M. Lifschitz, Fluid Mechanics, second ed., in: Course of Theoretical Physics, vol. 6, Pergamon Press, Oxford, 1989.
[22] F.F. Chen, Introduction to Plasma Physics and Controlled Fusion, vol. 1, second ed., Plenum Press, New York, 1990, 77.
[23] F.A. Haas, A. Thyagaraja, Conceptual and experimental bases of theory of anomalous transport in tokamaks, Phys. Rep. 143 (1986) 242.
[24] B.B. Kadomtsev, O.P. Pogutse, Electron heat conductivity of the plasma across a 'braided' magnetic field, in: Plasma Physics and Controlled Nuclear Fusion Research, I, Proc. 7th. Int. Conf. Innsbruck, IAEA Vienna, 1978, 1979, p. 649.
[25] A.B. Rechester, M.N. Rosenbluth, Electron heat transport in a tokamak with destroyed magnetic surfaces, Phys. Rev. Lett. 40 (1978) 38.
[26] T.B. Benjamin, Instability of periodic wavetrains in nonlinear dispersive systems, Proc. Roy. Soc. A 299 (1967) 59.
[27] E.N. Parker, A. Thyagaraja, The separation of field and fluid in the sun, Solar Phys. 189 (1999) 45.
[28] M.R. de Baar, A. Thyagaraja, P.J. Knight, G.M.D. Hogeweij, N.J. Lopes-Cardozo, Numerical simulations of turbulence in RTP discharges with dominant off-axis ECH, J. Plasma Fusion Res. Ser. 5 (2002) 318.